Spin Waves and Revised Crystal Structure of Honeycomb Iridate Na_2IrO_3

S. K. Choi,[1] R. Coldea,[1] A. N. Kolmogorov,[2] T. Lancaster,[1,*] I. I. Mazin,[3] S. J. Blundell,[1] P. G. Radaelli,[1] Yogesh Singh,[4,5] P. Gegenwart,[4] K. R. Choi,[6] S.-W. Cheong,[6,7] P. J. Baker,[8] C. Stock,[8] and J. Taylor[8]

[1]*Clarendon Laboratory, University of Oxford, Parks Road, Oxford OX1 3PU, United Kingdom*
[2]*Department of Materials, University of Oxford, Parks Road, Oxford OX1 3PH, United Kingdom*
[3]*Code 6393, Naval Research Laboratory, Washington, D.C. 20375, USA*
[4]*I. Physikalisches Institut, Georg-August-Universität Göttingen, D-37077 Göttingen, Germany*
[5]*Indian Institute of Science Education and Research Mohali, Sector 81, SAS Nagar, Manauli PO 140306, India*
[6]*l_PEM, Pohang University of Science and Technology, Pohang 790-784, Korea*
[7]*R-CEM and Department of Physics and Astronomy, Rutgers University, Piscataway, New Jersey 08854, USA*
[8]*ISIS Facility, Didcot, Oxfordshire, OX11 0QX, United Kingdom*

(Received 24 October 2011; published 20 March 2012)

We report inelastic neutron scattering measurements on Na_2IrO_3, a candidate for the Kitaev spin model on the honeycomb lattice. We observe spin-wave excitations below 5 meV with a dispersion that can be accounted for by including substantial further-neighbor exchanges that stabilize zigzag magnetic order. The onset of long-range magnetic order below $T_N = 15.3$ K is confirmed via the observation of oscillations in zero-field muon-spin rotation experiments. Combining single-crystal diffraction and density functional calculations we propose a revised crystal structure model with significant departures from the ideal 90° Ir-O-Ir bonds required for dominant Kitaev exchange.

DOI: 10.1103/PhysRevLett.108.127204 PACS numbers: 75.10.Jm, 61.72.Nn, 75.40.Gb, 76.75.+i

Transition metal oxides of the 5*d* group have recently attracted attention as candidates to exhibit novel electronic ground states stabilized by the strong spin-orbit (SO) coupling, including topological band or Mott insulators [1], quantum spin liquids [2], field-induced topological order [3], topological superconductors [4], and spin-orbital Mott insulators [5]. The compounds $\mathcal{A}_2IrO_3$ ($\mathcal{A}$ = Li, Na) [6,7], in which edge-sharing IrO_6 octahedra form a honeycomb lattice [see Fig. 1(b)], have been predicted to display novel magnetic states for composite spin-orbital moments coupled via frustrated exchanges. The exchange between neighboring Ir moments (called $\boldsymbol{S}_{i,j}$, $S = 1/2$) is proposed to be [2]

$$\mathcal{H}_{ij} = -J_K S_i^\gamma S_j^\gamma + J_1 \boldsymbol{S}_i \cdot \boldsymbol{S}_j, \qquad (1)$$

where $J_K > 0$ is an Ising ferromagnetic (FM) term arising from superexchange via the Ir-O-Ir bond, and $J_1 > 0$ is the antiferromagnetic (AFM) Heisenberg exchange via direct Ir-Ir 5*d* overlap. Because of the strong spin-orbital admixture the Kitaev term J_K couples only the components in the direction γ, normal to the plane of the Ir-O-Ir bond [2,8]. Because of the orthogonal geometry, different spin components along the cubic axes ($\gamma = x, y, z$) of the IrO_6 octahedron are coupled for the three bonds emerging out of each site in the honeycomb lattice. This leads to the strongly frustrated Kitaev-Heisenberg (KH) model [2], which has conventional Néel order for large J_1, a stripy collinear AFM phase (to be discussed later) for $0.4 \lesssim \alpha \lesssim 0.8$, where $\alpha = J_K/(J_K + 2J_1)$ (exact ground state at $\alpha = 1/2$), and a quantum spin liquid with Majorana fermion excitations [9] at large J_K ($\alpha \gtrsim 0.8$). In spite of many theoretical studies [2–4,10–13] very few experimental results are available for $\mathcal{A}_2IrO_3$ [6,7,14]. Evidence of unconventional magnetic order in Na_2IrO_3 came from resonant x-ray scattering [14] which showed magnetic Bragg peaks at wave vectors consistent with either an in-plane zigzag or stripy order (to be discussed later).

Measurements of the spin excitations are very important to determine the overall energy scale and the relevant magnetic interactions, however, because Ir is a strong neutron absorber inelastic neutron scattering (INS) experiments are very challenging. Using an optimized setup we here report the first observation of dispersive spin-wave excitations of Ir moments via INS. We show that the dispersion can be quantitatively accounted for by including substantial further-neighbor in-plane exchanges, which in turn stabilize zigzag order. To inform future *ab initio* studies of microscopic models of the interactions we combine single-crystal x-ray diffraction with density functional calculations to determine precisely the oxygen positions, which are a key in mediating the exchange and controlling the spin-orbital admixture via crystal field effects. We propose a revised crystal structure with much more symmetric IrO_6 octahedra, but with substantial departures from the ideal 90° Ir-O-Ir bonds required for dominant Kitaev exchange [8], and with frequent structural stacking faults. This differs from the currently adopted model, used by several band-structure calculations [13,14], with asymmetrically distorted IrO_6 octahedra, with Ir-O bonds differing in length by more than 20%, improbably large in the absence of any Jahn-Teller interaction, and with the shortest Ir-O bond length below 2 Å, highly unlikely for a large

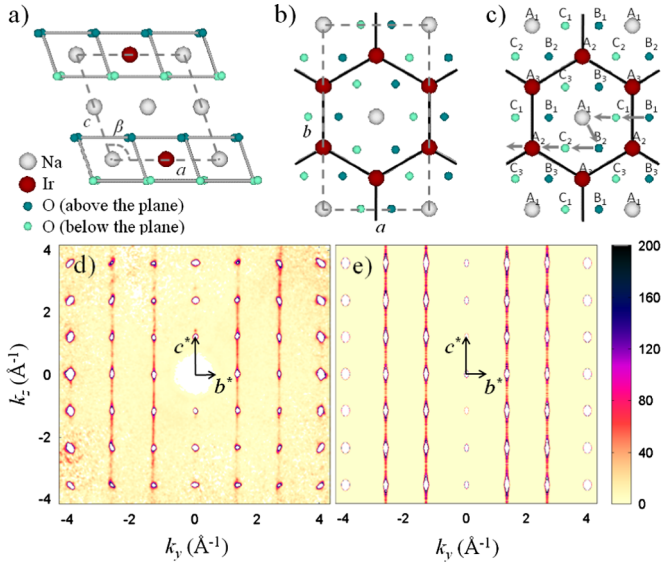

FIG. 1 (color online). (a) Layer stacking along the monoclinic c axis with an in-plane offset along a (dashed box is the $C2/m$ unit cell). (b) Basal layer ($z = 0$) showing the Ir honeycomb lattice. (c) Diagram to illustrate the layer stacking in the ideal honeycomb lattice. Ideal stacking of layers and stacking faults are explained in the text. (d) X-ray diffraction intensity in the (0, k, l) plane showing rods of diffuse scattering in between structural Bragg peaks along $\boldsymbol{c}^*$ with selection rule $h + k = 2n$ and $k = 3m + 1$ or $3m + 2$ (n, m integers) modeled in (e) by frequent in-plane translational stacking faults of the type shown by the thick arrows in (c).

ion such as Ir^{4+}. We show that the previously proposed structure is unstable with large unbalanced ionic forces, and when allowed to relax it converges to a higher-symmetry structure.

As other "213" honeycomb oxides, Na_2IrO_3 has an alternating stacking of hexagonal layers of edge-sharing NaO_6 octahedra and similar layers where two-thirds of Na are replaced by Ir to form a honeycomb lattice with Na in the center [see Fig. 1(b)]. To determine the precise structure x-ray diffraction was performed on a self-flux-grown single crystal of Na_2IrO_3 [6,15]. The diffraction pattern showed sharp Bragg peaks which could be indexed by a monoclinic unit cell [see Fig. 1(a)] derived from a parent rhombohedral structure with an ideal repeat every three layers. The monoclinic distortion leads to an in-plane shift of successive Ir honeycombs differing by 1.2% from the ideal value [$-c\cos\beta$ compared to $a/3$, see Fig. 1(a)], well above our instrumental resolution, which enabled us to determine that our sample was a single monoclinic domain. The detailed refinement [15] was performed using both the published $C2/c$ (No. 15) unit cell with 15 refined atomic positions leading to values somewhat similar to Ref. [6], and an alternative, higher-symmetry and half the unit cell volume, $C2/m$ model [No. 12, shown in Figs. 1(a) and 1(b)] (as found for the related Li_2IrO_3 [16]), with only seven refined atomic positions listed in Table I. Other

TABLE I. Structural parameters extracted from single-crystal x-ray data at 300 K. ($C2/m$ space group, $a = 5.427(1)$ Å, $b = 9.395(1)$ Å, $c = 5.614(1)$ Å, $\beta = 109.037(18)°$, $Z = 4$). All sites are fully occupied. U is the isotropic displacement. The goodness-of-fit was 2.887 ($R_{\rm int} = 0.1247$, $R_\sigma = 0.0584$) [15].

Atom	Site	x	y	z	U(Å^2)
Ir	$4g$	0.5	0.167(1)	0	0.001(1)
Na1	$2a$	0	0	0	0.001(6)
Na2	$2d$	0.5	0	0.5	0.009(7)
Na3	$4h$	0.5	0.340(2)	0.5	0.009(6)
O1	$8j$	0.748(6)	0.178(2)	0.789(6)	0.001(6)
O2	$4i$	0.711(7)	0	0.204(7)	0.001(7)

structural motifs reported for 213 honeycomb oxides [17] including Na_2PtO_3, Li_2TeO_3, Na_2TbO_3 were also tried but did not provide a good fit. We also tested for Ir/Na site admixture but this did not improve the agreement with data.

The $C2/c$ structure can be described as a "supercell" obtained from the $C2/m$ structure by small displacements of atoms (of the order of a few percent of the unit cell dimensions) leading to a doubled unit cell volume. Although $C2/m$ and $C2/c$ gave comparable agreement with the main Bragg peaks, the larger $C2/c$ unit cell should be manifested experimentally by the appearance of new "superstructure" peaks at positions such as (odd,odd,half-integer) in the small unit cell description ($C2/m$). These superlattice peaks, however, were not observed in the data [15], ruling out the $C2/c$ model. Furthermore, in structural optimization calculations using VASP [15,18] (also confirmed by an all-electron LAPW code [19]) we find that the $C2/c$ structural model, which has asymmetrically distorted IrO_6 octahedra, is unstable: (i) the forces on oxygen are very large, exceeding 3 eV/A for the published $C2/c$ cell [6] and (ii) when the structure is allowed to relax the oxygens move such as to recover the more symmetric $C2/m$ structure with the Ir-O distances converging to within 1.1% of the experimentally refined values in Table I. The IrO_6 octahedra are much more symmetric in the $C2/m$ model with Ir-O distances and Ir-O-Ir bond angles ranging from 2.06 to 2.08 Å, and 98° to 99.4°, respectively, compared to the wider ranges 1.99 to 2.43 Å, and 91° to 98° proposed before [6].

In addition to sharp Bragg peaks, visible diffuse "rods" of scattering were also observed [see Fig. 1(d)] and could be quantitatively understood [compare with calculation in Fig. 1(e)] in terms of a structural model that allows for the possibility of faults in the stacking sequence along the c axis. The stacking of atomic layers can be easily visualized with reference to projections in the basal plane [Fig. 1(c)], where A defines a nominal hexagonal lattice (made up of three triple-cell sublattices A_1-A_3), and B and C are also hexagonal lattices with positions in the center of a triangle of A sites. The atomic stacking is always in the

ABC sequence to minimize the interlayer Coulomb energy, i.e., Ir-O-Na-O-Ir-O is A_1-*B*-*C*-*A*-B_1-*C*. Only Ir layers have a sublattice index, indicating the position of the Na at the honeycomb center, as the other atomic layers are full hexagonal lattices. However, if neighboring Ir layers are only weakly interacting (as they are separated by a hexagonal NaO_2 layer) then the second Ir layer could be shifted to another position on the *B* lattice, say B_2 [thick arrows in Fig. 1(c)] or B_3, with only minimal energy cost, as that would not affect the bonding with the fully hexagonal NaO_2 layers below and above. To quantitatively verify this idea, we performed structural optimization calculations using VASP [15] in an extended unit cell to include a stacking fault of the type illustrated in Fig. 1(c) and found that the energy cost of a stacking fault is extremely small, below 0.1 meV/Å^2, explaining why such stacking faults are very likely to occur.

The calculated scattering for such a microscopic model [15] indeed reproduces well the selection rule for where diffuse scattering occurs in Figs. 1(d) and 1(e). In particular, there is no diffuse scattering along (00l), as this corresponds to adding all layers in phase irrespective of their in-plane translations. Also there is no diffuse scattering along (0, 6n, l) (n integer), as again layers add in phase because the two allowed in-plane translations have a phase factor equal to a multiple of 2π. We use the strength of the diffuse scattering integrated between (020) and (021) relative to the intensity of the (020) peak (to have similar absorption factor), obtained experimentally as $\simeq 0.42$, to estimate the probability for stacking faults $p \simeq 9\%$, this means that on average one fault occurs every $1/p \simeq 10$ layers. We measured over 30 crystals from a batch and all showed diffuse scattering, suggesting that this is a common structural feature.

The magnetic order of the Ir spins was detected by zero-field (ZF) muon-spin rotation (μ^+SR) on a powder sample of Na_2IrO_3. Example raw spectra are shown in Fig. 2(a). At temperatures below $T_N = 15.3$ K, we observe clear oscillations in the time dependence of the muon polarization,

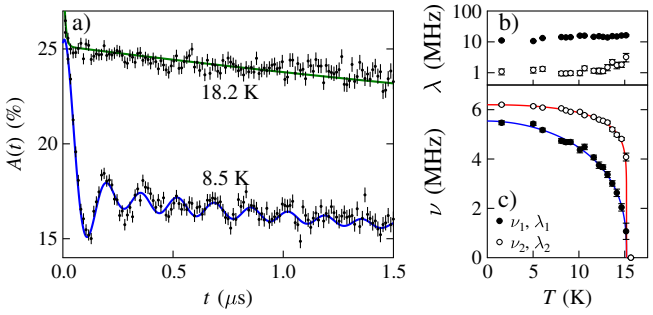

FIG. 2 (color online). (a) ZF μ^+SR spectra on a polycrystalline sample of Na_2IrO_3 above and below T_N. Solid lines are (top) a guide to the eye and (bottom) a fit described in the text. (b),(c) Fitted parameters as a function of temperature.

characteristic of quasistatic local magnetic fields at the muon stopping site. Fits to the time-dependent muon data reveal that two frequencies are present, indicating the presence of two distinct muon stopping sites with different local fields. The full spectra was fitted to the form $A(t) = A_1 e^{-\lambda_1 t}\cos(2\pi\nu_1 t + \phi_1) + A_2 e^{-\lambda_2 t}\cos(2\pi\nu_2 t + \phi_2) + A_3 e^{-\Lambda t} + A_{\mathrm{bg}}$, where the last two terms account for muons polarized parallel to the local magnetic fields, and muons stopping in the sample holder (or cryostat tail), respectively. Using our best-fit parameters we estimate that the muons occupy the two sites with a probability ratio of about 9:1. Both local fields set in at a common temperature, but have a distinctly different temperature dependence [see Fig. 2(b)]. The relative weight of the second frequency component suggests that it may come from muon sites implanted near stacking fault planes, as such sites also occur in a similar proportion. Our value for T_N is consistent with both susceptibility measurements on the same batch, which indicated a clear anomaly (sharp downturn) near T_N as reported previously [6,7], and the magnetic Bragg peaks observed in resonant x-ray scattering [14].

The magnetic excitations were probed by powder inelastic neutron scattering using the direct-geometry time-of-flight spectrometer MARI at ISIS with an optimized setup to minimize absorption [15]. Figure 3(e) shows the raw neutron scattering intensity as a function of wave vector ($Q = |\boldsymbol{Q}|$) and energy transfer deep in the ordered phase. An inelastic signal with a sinusoidal-like dispersive boundary below a maximum near 5 meV is clearly observed at low Q. A gap, if present is smaller than 2 meV. The magnetic character of the scattering is confirmed by the broad, damped-out signal observed in the paramagnetic phase at 55 K [see Figs. 3(f) and 3(g) (contrast filled and open symbols)]. Interestingly, the dispersion boundary extrapolates at the lowest energies to a wave vector Q much smaller than that expected for conventional Néel order, $Q_{(020)} = 1.34$ Å^{-1}, so this magnetic order can be ruled out; in fact Q is close to the expected location of the first magnetic Bragg peak for both zigzag or stripy order, $Q_{(010)} = 0.67$ Å^{-1}. Figures 3(h) and 3(i) show the calculated scattering from spin waves of a 2D Heisenberg model with up to third neighbor exchanges, $J_{1,2,3}$, with zigzag ($J_1 = 4.17$ meV, $J_2/J_1 = 0.78$, $J_3/J_1 = 0.9$) and stripy order ($J_1 = 10.89$ meV, $J_2/J_1 = 0.26$, $J_3/J_1 = -0.2$), respectively (we neglect the interlayer couplings believed to be small). The constraints to reproduce the dispersion maximum and the measured Curie-Weiss (CW) temperature [$\Theta = -S(S+1)(J_1 + 2J_2 + J_3)/k_B \sim -125$ K [7]] are not sufficient to determine all three exchanges, so the values chosen are *representative* of the level of agreement that can be obtained [15]. The calculation for the zigzag phase [Fig. 3(h)] can reproduce well the observed dispersion at low-Q (filled symbols), whereas the stripy phase [Fig. 3(i)] cannot account for the strong low-Q dispersive

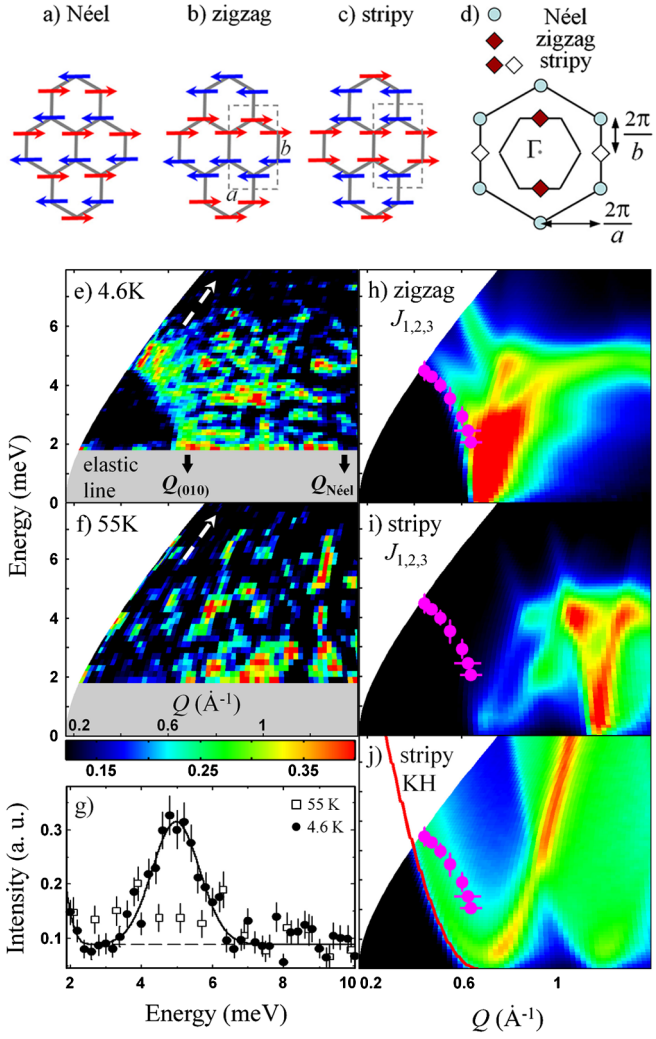

FIG. 3 (color online). Diagram of (a) Néel, (b) zigzag, and (c) stripy order. (d) Reciprocal space diagram showing locations of magnetic Bragg peaks for various magnetic phases (inner hexagon shows first Brillouin zone of the honeycomb lattice). (e) Powder inelastic neutron scattering data. The notable well-defined feature is the sharp lower boundary of the scattering at low Q [filled (magenta) symbols in (h)–(j)], which we associate with a sinusoidal spin-wave dispersion; this becomes damped out in the paramagnetic phase in (f). Slanted thick dashed arrow shows the scan direction in (g). Gray shading marks the inaccessible region close to the elastic line dominated by incoherent elastic scattering. (g) Energy scan (solid points 4.6 K, open symbols 55 K) through the maximum spin-wave energy seen in (e) fitted to a Gaussian peak (solid line), dashed line is estimated background. (h)–(j) Calculated spherically averaged spin-wave intensity [15] for the $J_{1,2,3}$ model with (h) zigzag or (i) stripy order, and (j) the KH model with stripy order for parameters given in the text. Solid red line in (j) highlights the low-energy boundary, which coincides with the dispersion from Γ to the first softening point.

signal and predicts stronger scattering at larger Q's not seen. Calculations for the KH Hamiltonian (1) are shown in Fig. 3(j) for $\alpha = 0.4$ (lower limit for the stripy phase) and $J_1 = 25.85$ meV to reproduce the CW temperature [20] $\Theta = -S(S+1)(J_1 - J_K/3)/k_B$. The lower boundary of the scattering at low Q (solid line) is predicted to have a quadratic shape near the first softening point, a robust feature for any α throughout the stripy phase. This is in contrast to the data where the dispersion boundary (marked by filled symbols) has a distinctly different, sinusoidal-like shape with a curvature the opposite way. In addition, a different distribution of scattering weight to higher energies is predicted, but not seen in the data. We conclude that the KH model in the stripy phase has a qualitatively different spin-wave spectrum compared to the data. A minimal model that can reproduce the observed low-Q dispersion and which predicts distribution of magnetic scattering in broad overall agreement with the data up to some intensity modulations is shown in Fig. 3(h) and requires substantial couplings up to third neighbors, which stabilize zigzag magnetic order. Recent theory [12] proposed that in addition to couplings up to third neighbors, a Kitaev term may also exist. We have compared the data with such a model as well [15] and estimate that a Kitaev term, if present, is smaller than an upper bound corresponding to $\alpha \lesssim 0.40(5)$.

We note that sizable J_3's are not uncommon in triangular plane metal oxides. The reason is that even though J_1 involves two hoppings and J_3 four, the two additional hoppings are strong $pd\sigma$ ones, and the hopping proceeds through intermediate unoccupied e_g states [21]. In the case of Na_2IrO_3 the hopping proceeds through somewhat higher Na s orbitals, but these are very diffuse, and the corresponding $t_{sp\sigma}$ parameter is sizable. Near cancellation of the AFM and FM superexchange interaction for the nearest-neighbor path further reduces J_1 compared to J_3.

To summarize, by combining single-crystal diffraction and local-density approximation calculations we proposed a revised crystal structure for the spin-orbit coupled honeycomb antiferromagnet Na_2IrO_3 that highlights important departures from the ideal case where the Kitaev exchange dominates. We observed dispersive spin-wave excitations in inelastic neutron scattering and showed that substantial further-neighbor exchange couplings are required to explain the observed dispersion and we proposed a model for the magnetic ground state that could support such a dispersion relation.

We thank G. Jackeli for providing notes on spin-wave dispersions for the KH model in the rotated frame, A. Amato for technical support, N. Shannon, J. T. Chalker, and L. Balents for discussions, and EPSRC for funding. Work at Rutgers was supported by DOE (DE-FG02-07ER46382).

Note added in proof.—Very recently, neutron diffraction data on single crystals of Na_2IrO_3 was reported, which also provided evidence in support of zigzag magnetic order, and x-ray studies obtained similar structural information [22].

*Present address: Department of Physics, Durham University, South Road, Durham DH1 3LE, United Kingdom.

[1] D. Pesin and L. Balents, Nature Phys. **6**, 376 (2010).
[2] J. Chaloupka, G. Jackeli, and G. Khaliullin, Phys. Rev. Lett. **105**, 027204 (2010).
[3] H. Jiang, Z. Gu, X. Qi, and S. Trebst, Phys. Rev. B **83**, 245104 (2011).
[4] Y-Z. You, I. Kimchi, and A. Vishwanath, arXiv:1109.4155.
[5] B. J. Kim, Hosub Jin, S. J. Moon, J.-Y. Kim, B.-G. Park, C. S. Leem, Jaejun Yu, T. W. Noh, C. Kim, S.-J. Oh, J.-H. Park, V. Durairaj, G. Cao, and E. Rotenberg, Phys. Rev. Lett. **101**, 076402 (2008); B. J. Kim, H. Ohsumi, T. Komesu, S. Sakai, T. Morita, H. Takagi, and T. Arima, Science **323**, 1329 (2009).
[6] Y. Singh and P. Gegenwart, Phys. Rev. B **82**, 064412 (2010).
[7] Yogesh Singh, S. Manni, J. Reuther, T. Berlijn, R. Thomale, W. Ku, S. Trebst, and P. Gegenwart, preceding Letter, Phys. Rev. Lett. **108**, 127203 (2012).
[8] G. Jackeli and G. Khaliullin, Phys. Rev. Lett. **102**, 017205 (2009).
[9] A. Kitaev, Ann. Phys. (N.Y.) **321**, 2 (2006).
[10] A. Shitade, H. Katsura, J. Kunes, X.-L. Qi, S.-C. Zhang, and N. Nagaosa, Phys. Rev. Lett. **102**, 256403 (2009).
[11] C. H. Kim, H. S. Kim, H. Jeong, H. Jin, and J. Yu, Phys. Rev. Lett. **108**, 106401 (2012).
[12] I. Kimchi and Y. Z. You, Phys. Rev. B **84**, 180407(R) (2011).
[13] S. Bhattacharjee, S-S. Lee, and Y. B. Kim, arXiv:1108.1806v2.
[14] X. Liu, T. Berlijn, W.-G. Yin, W. Ku, A. Tsvelik, Y.-J. Kim, H. Gretarsson, Y. Singh, P. Gegenwart, and J. P. Hill, Phys. Rev. B **83**, 220403(R) (2011).
[15] See Supplemental Material at http://link.aps.org/supplemental/10.1103/PhysRevLett.108.127204 for details.
[16] M. J. O'Malley, H. Verweij, and P. M. Woodward, J. Solid State Chem. **181**, 1803 (2008).
[17] Von W. Urland and R. Hoppe, Z. Anorg. Allg. Chem. **392**, 23 (1972); R. J. Kuban, Cryst. Res. Technol. **18**, 85 (1983); R. Wolf and R. Hoppe, Z. Anorg. Allg. Chem. **556**, 97 (1988).
[18] G. Kresse and J. Hafner, Phys. Rev. B **47**, 558 (1993); G. Kresse and J. Furthmüller, Phys. Rev. B **54**, 11 169 (1996).
[19] P. Blaha, K. Schwarz, G. Madsen, D. Kvasnicka, and J. Luitz, *WIEN2K* (T. U. Wien, Austria, 2002).
[20] J. Reuther, R. Thomale, and S. Trebst, Phys. Rev. B **84**, 100406(R) (2011).
[21] I. I. Mazin, Phys. Rev. B **76**, 140406(R) (2007).
[22] F. Ye, S. Chi, H. Cao, B. C. Chakoumakos, J. A. Fernandez-Baca, R. Custelcean, T. Qi, O. B. Korneta, and G. Cao, arXiv:1202.3995.